THE JOURNAL OF BIOLOGICAL CHEMISTRY VOL. 290, NO. 32, pp. 19796–19805, August 7, 2015

Identification of the Docking Site for CD3 on the T Cell Receptor β Chain by Solution NMR*

Received for publication, May 6, 2015, and in revised form, June 9, 2015 Published, JBC Papers in Press, June 24, 2015, DOI 10.1074/jbc.M115.663799

Yanan He[‡§1], Sneha Rangarajan[‡¶1], Melissa Kerzic[‡], Ming Luo[‡‖2], Yihong Chen[‡], Qian Wang[‡], Yiyuan Yin[‡], Creg J. Workman[**], Kate M. Vignali[**], Dario A. A. Vignali[**], Roy A. Mariuzza[‡¶3], and John Orban[‡§4]

*From the [‡]W. M. Keck Laboratory for Structural Biology, University of Maryland Institute for Bioscience and Biotechnology Research, Rockville, Maryland 20850, the Departments of [§]Chemistry and Biochemistry and [¶]Cell Biology and Molecular Genetics, University of Maryland, College Park, Maryland 20742, the [‖]Hefei National Laboratory for Physical Sciences at Microscale and School of Life Sciences, University of Science and Technology of China, Hefei, Anhui 230027, China, and the **Department of Immunology, University of Pittsburgh School of Medicine, Pittsburgh, Pennsylvania 15261*

Background: Understanding T cell signaling requires knowing the structure of the TCR-CD3 complex.
Results: Solution NMR was used to identify the docking site for CD3 ectodomains on the TCR β chain.
Conclusion: The docking site (~400 Å^2) comprises ~10 Cβ residues at the base of the TCR.
Significance: CD3 is located opposite to the peptide-MHC binding site of the TCR.

The T cell receptor (TCR)-CD3 complex is composed of a genetically diverse αβ TCR heterodimer associated noncovalently with the invariant CD3 dimers CD3εγ, CD3εδ, and CD3ζζ. The TCR mediates peptide-MHC recognition, whereas the CD3 molecules transduce activation signals to the T cell. Although much is known about downstream T cell signaling pathways, the mechanism whereby TCR engagement by peptide-MHC initiates signaling is poorly understood. A key to solving this problem is defining the spatial organization of the TCR-CD3 complex and the interactions between its subunits. We have applied solution NMR methods to identify the docking site for CD3 on the β chain of a human autoimmune TCR. We demonstrate a low affinity but highly specific interaction between the extracellular domains of CD3 and the TCR constant β (Cβ) domain that requires both CD3εγ and CD3εδ subunits. The mainly hydrophilic docking site, comprising 9–11 solvent-accessible Cβ residues, is relatively small (~400 Å^2), consistent with the weak interaction between TCR and CD3 extracellular domains, and devoid of glycosylation sites. The docking site is centered on the αA and αB helices of Cβ, which are located at the base of the TCR. This positions CD3εγ and CD3εδ between the TCR and the T cell membrane, permitting us to distinguish among several possible models of TCR-CD3 association. We further correlate structural results from NMR with mutational data on TCR-CD3 interactions from cell-based assays.

T cells play a major role in generating adaptive immune responses to microbes and cancers. This process is mediated by the T cell receptor (TCR)[5]-CD3 complex, which is composed of a genetically diverse αβ (or γδ) TCR heterodimer in noncovalent association with invariant CD3 dimers: CD3εγ, CD3εδ, and CD3ζζ (1, 2). The TCR recognizes antigenic peptides presented by major histocompatibility complex (MHC) molecules, whereas the CD3 subunits transmit activation signals to the T cell. The TCR α and β chains do not possess intracellular signaling motifs, thereby separating peptide-MHC (pMHC) recognition from T cell activation. By contrast, the CD3 ε, γ, δ, and ζ chains each contain at least one immunoreceptor tyrosine-based activation motif (ITAM). The TCR-CD3 complex exists in 1:1:1:1 stoichiometry for the TCRαβ/CD3εγ/CD3εδ/CD3ζζ dimers (3).

X-ray crystallographic studies of TCR-pMHC complexes have revealed the molecular basis for TCR recognition of foreign antigens and self-antigens (4–8). In addition, much is known about the downstream signaling cascade, following phosphorylation of CD3 ITAMs by the Src kinase Lck associated with CD4 or CD8 (9). However, the mechanism(s) by which TCR ligation is communicated to the CD3 signaling apparatus remains a mystery (10, 11). A critical missing element to solving this puzzle is knowledge of the spatial organization of the TCR-CD3 complex and the precise interactions between TCR and CD3 subunits. Although structures of the immunoglobulin (Ig)-like ectodomains of isolated CD3εγ and CD3εδ heterodimers have been determined (12–15), exactly how these

* This work was supported, in whole or in part, by National Institutes of Health Grants AI101911 (to J. O. and R. A. M.), AI036900 (to R. A. M.), and AI52199 (to D. A. A. V.). The NMR facility is jointly supported by the University of Maryland, the National Institute of Standards and Technology, and a grant from the W. M. Keck Foundation. The authors declare that they have no conflicts of interest with the contents of this article.
[1] Both authors contributed equally to this work.
[2] Supported by the joint supervision Ph.D. Project of the China Scholarship Council.
[3] To whom correspondence may be addressed: University of Maryland Institute for Bioscience and Biotechnology Research, 9600 Gudelsky Dr., Rockville, MD 20850. Tel.: 240-314-6243; Fax: 240-314-6225; E-mail: rmariuzz@umd.edu.
[4] To whom correspondence may be addressed: University of Maryland Institute for Bioscience and Biotechnology Research, 9600 Gudelsky Dr., Rockville, MD 20850. Tel.: 240-314-6221; Fax: 240-314-6225; E-mail: jorban@umd.edu.

[5] The abbreviations used are: TCR, T cell receptor; pMHC, peptide-MHC; ITAM, immunoreceptor tyrosine-based activation motif; SAXS, small angle x-ray scattering; ECD, extracellular domain; MBP, myelin basic protein; scFv, single-chain Fv; V, TCR variable domain; C, TCR constant domain; IRES, internal ribosome entry site.

subunits associate with TCR on the T cell surface remains to be established.

A variety of approaches have been used to infer the stoichiometry, pairing, and orientation of subunits within the TCR-CD3 complex. For example, mutational studies have demonstrated the importance of conserved charged residues in the transmembrane helices of the TCR and CD3 chains for complex assembly (1, 16). The following pairings have been established: TCRα-CD3$\epsilon\delta$, TCRα-CD3$\zeta\zeta$, and TCRβ-CD3$\epsilon\gamma$. Besides these transmembrane interactions, extracellular interactions between the TCR and the Ig-like ectodomains of CD3$\epsilon\gamma$ and CD3$\epsilon\delta$ also contribute to the structural integrity and function of the TCR-CD3 complex (2, 11, 17–21). By contrast, the ectodomain of CD3ζ, which is only 9 residues long, has not been implicated in interactions with the TCR. Although possible docking sites on the TCR for CD3 subunits have been proposed (18–20), these key interaction regions remain undefined.

Recently, small angle x-ray scattering (SAXS) was applied to a soluble TCR-CD3$\epsilon\delta$ complex that was engineered for stability by replacing the transmembrane domains with a heterotrimeric coiled coil (22). The SAXS results indicated that the extracellular domains (ECDs) of CD3$\epsilon\delta$ are situated underneath the TCR α chain, although a docking site was not identified. This arrangement was consistent with negative stain electron microscopy (EM) of the entire TCR-CD3 integral membrane complex, which further showed that the CD3$\epsilon\gamma$ ECDs sit beneath the TCR β chain (22). Intriguingly, EM images revealed mainly dimeric complexes in which two TCRs projected outward from a central core composed of the CD3 ECDs.

Although SAXS and negative stain EM have provided important information on the overall organization of the TCR-CD3 complex, these structural techniques lack the resolution necessary to establish the precise orientation of TCR and CD3 subunits in the complex or to define TCR-CD3 interfaces. At present, such information can only come from x-ray crystallography, NMR, or cryo-EM, applied individually or in combination. However, efforts to crystallize TCR-CD3 complexes have been thwarted by the very low affinity of TCR-CD3 interactions in solution. Similarly, previous attempts to map binding epitopes by NMR were unable to detect an interaction between TCR and CD3 ECDs (14). Using optimized protein constructs and isotope labeling conditions, we have revisited the application of NMR to define TCR-CD3 contact sites in solution. Here we demonstrate a specific interaction between TCR and CD3$\epsilon\gamma$ and CD3$\epsilon\delta$ ECDs by NMR, identify the docking site for CD3 on the TCR β chain, and correlate our structural results with mutational data on TCRβ-CD3 interactions from cell-based assays.

Experimental Procedures

Production and Purification of CD3$\epsilon\gamma$ and CD3$\epsilon\delta$ Heterodimers—Human CD3$\epsilon\gamma$ and CD3$\epsilon\delta$ heterodimers were prepared by *in vitro* folding from inclusion bodies produced in *Escherichia coli*. CD3$\epsilon\delta$ needed to be folded together with the anti-CD3ϵ antibody UCHT1 in order to form a stable species (15). By contrast, the CD3$\epsilon\gamma$ heterodimer was stable on its own. DNA fragments encoding the ECDs of CD3ϵ (residues 1–105), CD3γ (residues 1–90), and CD3δ (residues 1–79) were inserted separately into the vector pET-26b (Novagen) and expressed as inclusion bodies in BL21(DE3) *E. coli* cells (Novagen). The UCHT1 antibody was likewise produced in inclusion bodies as a single-chain Fv fragment (scFv) in which the light chain variable region was connected to the heavy chain variable region by a $(GGGGS)_3$ linker. Bacteria were grown at 37 °C in LB medium to $A_{600} = 0.6–0.8$ and induced with 1 mM isopropyl-β-D-thiogalactoside. After incubation for 3 h, the bacteria were harvested by centrifugation and resuspended in 50 mM Tris-HCl (pH 8.0) containing 0.1 M NaCl and 2 mM EDTA; cells were disrupted by sonication. Inclusion bodies were washed extensively with 50 mM Tris-HCl (pH 8.0) and 2% (v/v) Triton X-100. The CD3ϵ, CD3γ, and CD3δ chains were dissolved in 8 M urea, 50 mM Tris-HCl (pH 8.0), and 10 mM DTT; UCHT1 scFv was dissolved in 6 M guanidinium HCl, 100 mM Tris-HCl (pH 8.0), and 10 mM DTT.

For *in vitro* folding of CD3$\epsilon\gamma$, solubilized CD3ϵ and CD3γ inclusion bodies were rapidly diluted into ice-cold folding buffer containing 0.8 M arginine HCl, 50 mM Tris-HCl (pH 8.0), 2 mM EDTA, 3.7 mM cystamine, and 6.6 mM cysteamine to final protein concentrations of 59 and 52 mg/liter, respectively. For *in vitro* folding of scFv-CD3$\epsilon\delta$, CD3ϵ, CD3δ, and scFv inclusion bodies were diluted into the same buffer at final concentrations of 59, 45, and 130 mg/liter, respectively. After 72 h at 4 °C, the folding mixtures were concentrated 50-fold, dialyzed overnight against 20 mM Tris-HCl (pH 8.0) and 100 mM NaCl, and centrifuged to remove aggregates. Correctly folded CD3$\epsilon\gamma$ and scFv-CD3$\epsilon\delta$ proteins were then purified using sequential Superdex S-200 and MonoQ columns (GE Healthcare).

Production of TCR MS2-3C8 with Isotope-labeled β Chain—The β chain of TCR MS2-3C8 (residues 1–244) with U-^{2}H,^{13}C,^{15}N labeling was obtained by inclusion body expression in *E. coli* BL21(DE3) cells (Agilent) transformed with pET-26b. Transformed cells were grown in 25 ml of LB medium containing 30% D_2O (Isotec) at 37 °C until $A_{600} \geq 1.0$ and then transferred in a 1:50 dilution to 25 ml of M9 medium containing 70% D_2O, 1 g/liter [^{15}N]NH_4Cl (Cambridge Isotope) as the sole source of nitrogen and 4 g/liter [^{2}H,^{13}C]glucose (Cambridge Isotope) as the sole source of carbon. The culture was grown until $A_{600} = 0.5–1.0$ and was transferred in a 1:100 dilution to 100 ml of M9 containing 100% D_2O and grown overnight. The overnight cultures were used to inoculate 1 liter of M9/D_2O to a starting of $A_{600} = 0.10$. Induction with isopropyl-β-D-thiogalactoside to a final concentration of 1 mM was performed at $A_{600} \geq 0.6$, and growth was continued for 3–4 h at 37 °C. The bacteria were disrupted by sonication. Inclusion bodies were washed with and without 5% (v/v) Triton X-100 and then solubilized in 8 M urea, 50 mM Tris-HCl (pH 8.0), and 10 mM DTT.

The unlabeled TCR MS2-3C8 α chain (residues 1–205) was expressed as inclusion bodies in *E. coli* BL21(DE3) cells transformed with pET-26b. Bacteria were grown at 37 °C in LB medium to $A_{600} = 0.5–1.0$ and induced with 1 mM isopropyl-β-D-thiogalactoside. The inclusion bodies were washed with 5% (v/v) Triton X-100 and dissolved in 8 M urea, 50 mM Tris-HCl (pH 8.0), and 10 mM DTT.

For *in vitro* folding, the TCR MS2-3C8 α and β chains were mixed in a 3.6:1 molar ratio and diluted into a folding mixture containing 5 M urea, 0.4 M L-arginine HCl, 5 mM EDTA, 3.7

cystamine dihydrochloride, and 6.6 mM cysteamine to a final concentration of 50 mg/liter. The folding mixture was dialyzed against H_2O for 72 h at 4 °C and then dialyzed against 10 mM Tris-HCl (pH 8.0) for 48 h at 4 °C. After removal from dialysis, the folding mixture was concentrated and dialyzed against 50 mM MES (pH 6.0) at 4 °C overnight. Disulfide-linked TCR MS2-3C8 heterodimer was purified using sequential MonoQ and Superdex S-200 columns.

A U-^{2}H,^{15}N-labeled MS2-3C8 β chain with U-^{13}C, ^{15}N-labeled Ile, Leu, and Val was produced as described above. [^{1}H,^{12}C]glucose (Sigma) was used as the sole carbon source, and 50 mg/liter of each labeled amino acid (Sigma/Isotec) was added to M9/D2O 1 h prior to induction. A U-^{2}H,^{15}N-labeled MS2-3C8 β chain for titration experiments was produced similarly except for the use of [^{1}H,^{12}C]glucose as the sole carbon source.

NMR Spectroscopy—TCR MS2-3C8α[β-^{2}H,^{13}C,^{15}N] sample concentrations in the range of 200–240 μM were used in 50 mM NaP_i, 100 mM NaCl (pH 7.0) with the addition of 0.1 mg/ml Pefabloc (Sigma). NMR spectra were acquired at 25 °C on Bruker AVANCE III 600 and 900 Hz spectrometers fitted with Z-gradient ^{1}H/^{13}C/^{15}N cryoprobes. Backbone resonance assignment was carried out with TROSY versions of the following standard three-dimensional triple resonance experiments: HNCACB, HN(CO)CACB, HNCA, HN(CO)CA, HN(CA)CO, and HNCO. The HNCACB and HN(CO)CACB experiments were also recorded with optimization on the C$^{\beta}$ signals. Three-dimensional spectra were acquired using non-uniform sampling (25%) and reconstructed employing the method of Hyberts *et al.* (23). Three-dimensional HNCO, HN(CA)CO, HN(CO)CA, and HNCA experiments were also recorded on an MS2-3C8 sample where the β chain was deuterated and selectively [^{13}C,^{15}N]Ile/Leu/Val(ILV)-labeled. NMR spectra were processed using NMRPipe (24) and analyzed with SPARKY (25).

NMR titration experiments were carried out at 25 °C using 100 μM MS2-3C8α[β-^{2}H,^{15}N] and either unlabeled CD3$\epsilon\gamma$, scFv-CD3$\epsilon\delta$, or CD3$\epsilon\gamma$ plus scFv-CD3$\epsilon\delta$. Samples were exhaustively exchanged into identical buffer conditions (50 mM NaP_i, 100 mM NaCl, 0.1 mg/ml Pefabloc, pH 7.0) prior to titration. Unlabeled CD3 samples (typically 50 μM in 0.8–2.4 ml of buffer) were added to 200 μl of 100 μM labeled TCR and concentrated back to 200 μl using Centricon membrane filtration. In each titration, a two-dimensional ^{1}H-^{15}N HSQC spectrum was acquired for the MS2-3C8 TCR alone followed by spectra of successive CD3 additions. The following molar ratios were used for titrations: MS2-3C8/CD3$\epsilon\gamma$, 1:2, 1:4, and 1:5.8; MS2-3C8/scFv-CD3$\epsilon\delta$, 1:2 and 1:3.3; MS2-3C8/CD3$\epsilon\gamma$/scFv-CD3$\epsilon\delta$, 1:2:2, 1:4:4, and 1:6:6. Chemical shift perturbations were determined from $\Delta\delta_{total} = [(W_H\Delta\delta_H)^2 + (W_N\Delta\delta_N)^2]^{1/2}$, where $\Delta\delta_H$ and $\Delta\delta_N$ represent ^{1}H and ^{15}N chemical shift differences, respectively, between free and CD3-bound states of MS2-3C8, with weighting factors of $W_H = 1$ and $W_N = 0.2$. Values of $\Delta\delta_{total}$ above 0.01 ppm were estimated to be significant based on errors in the two-dimensional ^{1}H-^{15}N HSQC measurement of chemical shifts in multiple identical MS2-3C8 samples. Experimentally significant decreases in peak intensity were estimated as being above the average peak intensity decrease plus one S.D. value.

Generation of TCR-CD3 Mutants—A CD3 multicistronic construct containing CD3ϵ^{WT}, CD3δ^{WT}, CD3ζ^{WT}, and CD3γ^{WT} and an AND TCR multicistronic vector containing TCRα^{WT} and TCRβ^{WT} were generated as described previously (26–28). Briefly, the 2A peptide-linked CD3 and AND TCR constructs were generated by recombinant PCR and cloned into pMIG and pMIA, respectively (MSCV-based retroviral vectors containing an IRES-GFP or IRES-Ametrine1.1 (Addgene) cassette). Specific mutations in TCRβ (V166R, T199R, N203R, and R205E) were made by recombinant PCR, and subsequent mutant constructs were generated by appropriate subcloning.

TCR-CD3 Expression Analysis in HEK-293T Cells—Transient transfection of HEK-293T cells was performed as described previously with some modifications (29). HEK-293T cells were incubated in 6-well plates at 2×10^5/well overnight at 37 °C. The AND TCR$\alpha\beta$ pMIA plasmid (0.3 μg) and CD3 pMIG plasmid (0.3 μg) were transfected into HEK-293T cells using 6 μl of TransIT LT1 transfection reagent (Mirus). Cells were harvested 48 h after transfection and stained with anti-CD3ϵ and anti-TCRβ monoclonal antibodies for flow cytometric analysis.

Results

NMR Assignment of TCR MS2-3C8α[β-^{2}H,^{13}C,^{15}N]—For detailed NMR studies, we used a human autoimmune TCR, MS2-3C8, which recognizes a self-peptide from myelin basic protein (MBP) and the multiple sclerosis-associated MHC class II molecule HLA-DR4 (30). The pathogenic potential of MS2-3C8 was demonstrated using mice transgenic for this TCR and HLA-DR4 (31). An x-ray crystal structure of TCR MS2-3C8 bound to its pMHC ligand, MBP-HLA-DR4, has been determined (30), as well as that of the ternary complex formed by MS2-3C8, MBP-HLA-DR4, and CD4 (32). The interactions of MS2-3C8 with several of the key players in T cell signaling are therefore well characterized structurally, making this TCR a good candidate for studying critical associations with CD3$\epsilon\gamma$ and CD3$\epsilon\delta$. The MS2-3C8 TCR employed here was modified slightly from the wild-type used for previous x-ray studies, with three mutations in the α chain and four mutations in the β chain. The mutations were made to improve either expression (VβT55A), folding yield, and stability (CαT159C, CαC206(deleted), CβS171C, CβS189A, and CβC245(deleted)) or binding to HLA-DR4 (VαA31T). None of these mutations are at positions that contact CD3 (see below). Thus, the TCR MS2-3C8 ectodomain studied here is a heterodimer consisting of an unlabeled 205-residue α chain and a ^{2}H,^{13}C,^{15}N-labeled 244-residue β chain for a total molecular mass of ~50 kDa. Due to this relatively high molecular mass, transverse relaxation-optimized (TROSY)-based triple resonance experiments were utilized for the NMR assignment process (33). Interresidue connectivities were obtained through sequential matching of C$^{\alpha}$ and C$^{\beta}$ chemical shift patterns and confirmed with CO correlations in most cases. A selectively labeled ILV sample provided further validation of the assignments using methods described previously (34). Overall, 200 (87%) of the 230 possible main chain amide assignments were obtained, with extensive coverage of both TCR variable β (Vβ) and constant β (Cβ) domains (Fig. 1, *A–D*). Assignments of H^{N}, ^{15}N, C$^{\alpha}$, C$^{\beta}$, and CO

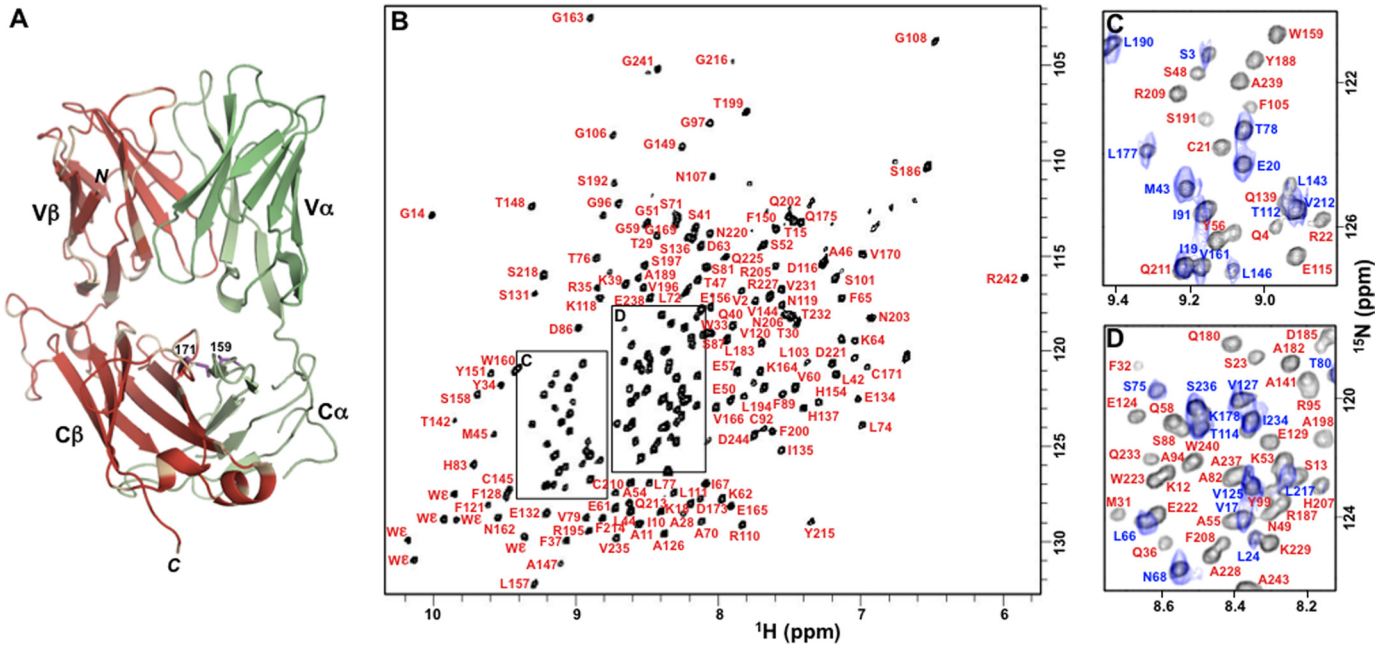

FIGURE 1. **NMR assignment of the TCR ectodomain MS2-3C8α[β-^{2}H,^{13}C,^{15}N].** *A*, extent of backbone amide assignments for the TCR β chain mapped onto the MS2-3C8 x-ray structure. Assigned regions of the β chain are shown in *red*, whereas unassigned regions are shown in *gray*. The α chain is in *green*. The sites of the CαT159C and CβS171C mutations to form an interchain disulfide (see "Results") are *highlighted* in *magenta*. *B*, two-dimensional ^{1}H-^{15}N TROSY-HSQC spectrum of MS2-3C8α[β-^{2}H,^{13}C,^{15}N] at 25 °C with backbone amide assignments. *C* and *D*, expanded regions from *B* with assignments. A two-dimensional HNCA spectrum of MS2-3C8α[β-^{2}H;ILV-^{13}C,^{15}N] (*blue*) is superimposed on the two-dimensional HSQC spectrum (*black*). *Peaks labeled* in *blue* are due to ILV residues or residues with an (i − 1) ILV.

resonances of the MS2-3C8α[β-^{2}H,^{13}C,^{15}N] sample have been deposited in the Biological Magnetic Resonance Bank (BMRB accession code 26569).

TCR MS2-3C8 β Chain Conformation and Dynamics in Solution—Chemical shift index analysis (35) using the assigned C^{α}, C^{β}, and CO resonances identified the secondary structure elements for the MS2-3C8 β chain in solution (Fig. 2*A*). These results were compared with the x-ray structure of MS2-3C8 in complex with MBP-HLA-DR4 (Protein Data Bank accession code 3O6F) (30). The only region that appears to be slightly different is strand D in the Cβ domain, which is a short 3-residue β-strand in the x-ray structure but has a coil conformation in solution. Interestingly, this is the region where we engineered a CαCys^{159}-CβCys^{171} interchain disulfide (36) to increase yields of paired TCR αβ heterodimers for the NMR sample. The wild-type protein used for x-ray analysis did not contain this disulfide (30). Generally, however, the secondary structure elements derived from chemical shifts are very similar to those observed in the x-ray structure, indicating comparable fold topologies for MS2-3C8 in solution and crystal forms. The chemical shift data were also used to obtain insights into the flexibility of the β chain in the context of the TCR αβ heterodimer (37). Thus, the high order parameters (S^2) for residues in the β chain of MS2-3C8 correspond with more rigid secondary structure elements, whereas lower values reflect less structured and more mobile loop regions (Fig. 2*B*). Moreover, most high S^2 regions in MS2-3C8 correlate with the lower temperature (*B*) factors of more ordered regions in the x-ray structure of the MS2-3C8-MBP-HLA-DR4 complex (Fig. 2, *B* and *C*). There are two notable exceptions, however. First, the complementarity-determining region loops have low S^2 values, consistent with being disordered in the free MS2-3C8 in solution, but have low *B* factors, consistent with order in the x-ray structure. This difference between the NMR and x-ray observations is to be expected because complexation with MBP-HLA-DR4 in the x-ray study rigidifies the complementarity-determining region loops, whereas the MS2-3C8 is uncomplexed in the solution NMR study. Second, there is a distinct difference between the main chain mobility inferred from order parameters *versus B* factors for the two α-helical regions in the Cβ domain, αA and αB (Fig. 2, *B* and *C*). For MS2-3C8 alone in solution, the relatively high S^2 values (~0.9) indicate that αA and αB are ordered α-helices. In contrast, these structured helical regions have high *B* factors (~120–140) in the x-ray structure of the MS2-3C8-MBP-HLA-DR4 complex, indicating increased mobility relative to other secondary structured regions in the complex. The differences in main chain flexibility of the αA and αB helices in free and pMHC-bound states are discussed further below.

TCR MS2-3C8 Interactions with CD3 ECDs—Unlabeled samples of recombinant CD3εγ and scFv-CD3εδ were checked for proper folding using one-dimensional ^{1}H NMR and circular dichroism spectra. ^{15}N-Labeled samples were also prepared, and two-dimensional ^{1}H-^{15}N HSQC spectra indicated well folded proteins (Fig. 3). The addition of unlabeled CD3εγ to MS2-3C8α[β-^{2}H,^{15}N] gave minimal chemical shift perturbations, even at the highest TCR/CD3εγ molar ratio of 1:5.8 (Fig. 4, *A* and *B*). Most shifts in the NMR spectrum had $\Delta\delta_{total}$ values less than 0.01 ppm, which is within the estimated experimental error of measurement. The few small changes that did occur were mainly due to residues in the Cβ domain, in the αA and αB helical regions and adjoining loops. Similarly, very few differ-

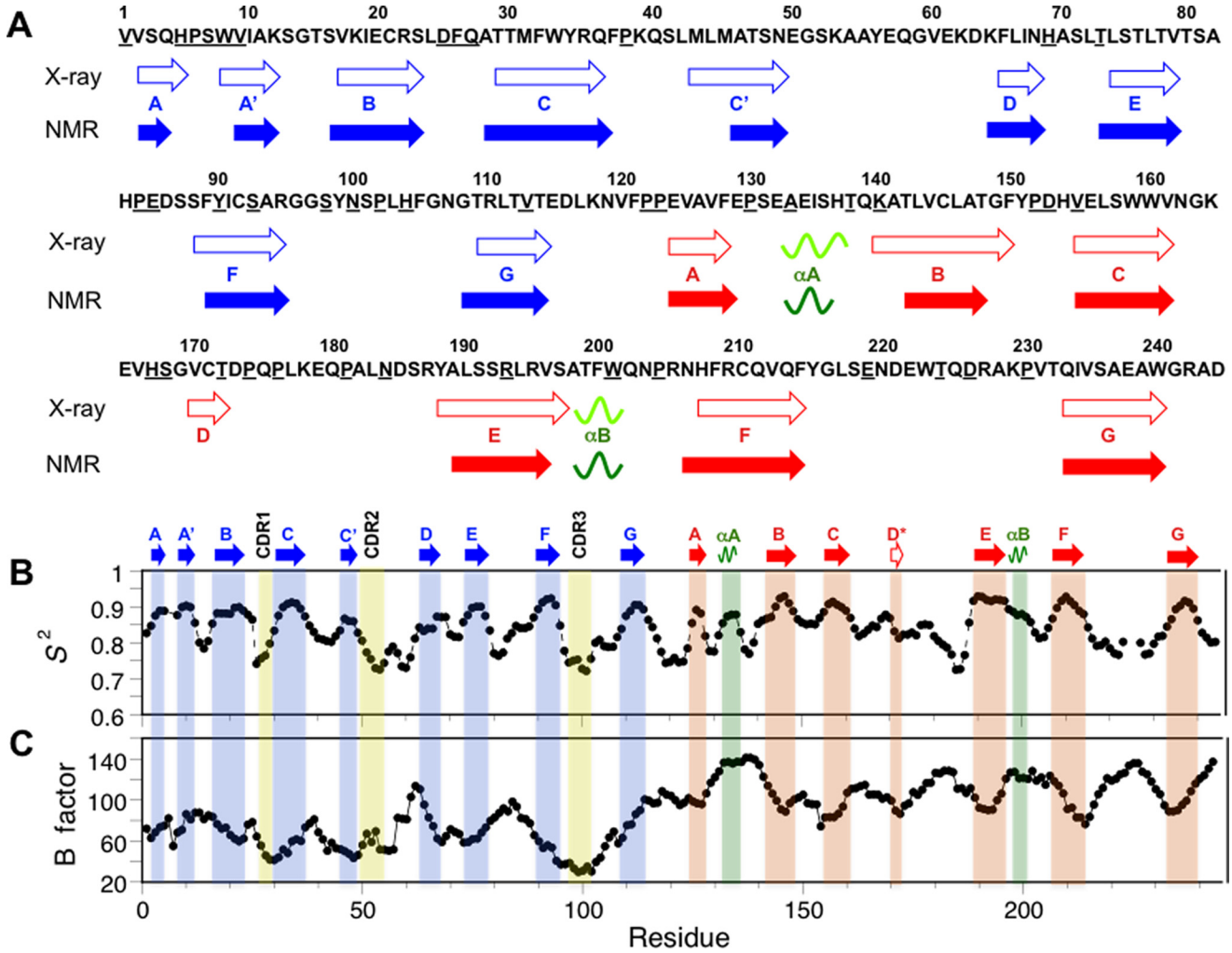

FIGURE 2. **Secondary structure and main chain flexibility of the β chain of $\alpha\beta$ TCR MS2-3C8 in solution.** *A*, comparison of secondary structure elements from x-ray (Protein Data Bank accession code 3O6F) and NMR data. The Vβ and Cβ domains are *colored blue* and *red*, respectively. Residues for which backbone amide assignments were not obtained, including prolines and the N-terminal amino acid, are *underlined*. *B*, estimated order parameters (S^2) from chemical shift data as a function of residue number. Secondary structured and other regions of interest are *highlighted* as follows: β-strands in the Vβ domain (*blue*), β-strands in the Cβ domain (*red*), α-helices in the Cβ domain (*green*), and complementarity-determining region (*CDR*) loops in the Vβ domain (*yellow*). *C*, temperature *B* factors for C$^{\alpha}$ atoms in the β chain of the MS2-3C8-MBP-HLA-DR4 complex (30). Regions are *highlighted* as in *B*.

ences in the MS2-3C8α[β-^{2}H,^{15}N] NMR spectrum resulted when only unlabeled scFv-CD3$\epsilon\delta$ was added. The largest change ($\Delta\delta_{total}$ ~0.013 ppm) corresponded to Arg^{195} in the Cβ domain, a residue that is at the interface with the Cα domain (Fig. 4, *A* and *B*). In contrast to the titrations with separate CD3 ECDs, the binding experiments where CD3$\epsilon\gamma$ and scFv-CD3$\epsilon\delta$ were added together to MS2-3C8α[β-^{2}H,^{15}N] produced more extensive chemical shift perturbations. In this case, 32 residues gave $\Delta\delta_{total}$ values ranging from 0.01 to 0.045 ppm (Fig. 4, *A* and *B*) such that 4 were in the Vβ domain and 28 were in the Cβ domain. These changes are consistent with a low affinity but highly specific interaction between CD3 ECDs and the TCR β chain, where only a subset of the NMR peaks are affected upon ligand binding. Moreover, the finding that both CD3$\epsilon\gamma$ and CD$\epsilon\delta$ must be added together to produce significant chemical shift perturbations suggests that the CD3 ECDs bind cooperatively to the TCR.

Control experiments were also carried out where two-dimensional ^{1}H-^{15}N HSQC spectra were acquired at different TCR concentrations ranging from 75 to 250 μM. Almost all of the TCR β chain residues have backbone amide chemical shifts that are invariant ($\Delta\delta_{total} \leq 0.005$ ppm) over this range, with a few exceptions in the Vβ domain. The largest $\Delta\delta_{total}$ value in these control experiments was for His^{83} (~0.03 ppm) with smaller values (0.005–0.01 ppm) for Met^{45}, Asp^{86}, Gly^{96}, and Gly^{97}. The chemical shift perturbations observed for these residues in the CD3 titrations may therefore have some contribution from small changes in TCR concentration-dependent effects.

Mapping of the most perturbed residues onto the x-ray structure of MS2-3C8 showed significant clustering in the Cβ domain, particularly in the αA and αB helices and neighboring residues, strongly suggesting that this region contains the binding epitope for CD3 (Fig. 5, *A* and *B*). Analysis of peak intensities indicated that decreases were uneven as CD3$\epsilon\gamma$ and scFv-CD3$\epsilon\delta$ were added, with larger losses corresponding to the two α-helices in the Cβ domain, αA and αB (Fig. 4*C*). Such disproportionate and localized decreases in peak intensity are indicative of binding interactions and provide further support for the chemical shift perturbation data. Based on the intensity changes, a K_D was estimated for the interaction between MS2-3C8 and CD3$\epsilon\gamma$/$\epsilon\delta$ of ~320 $\pm$ 100 μM (Fig. 6).

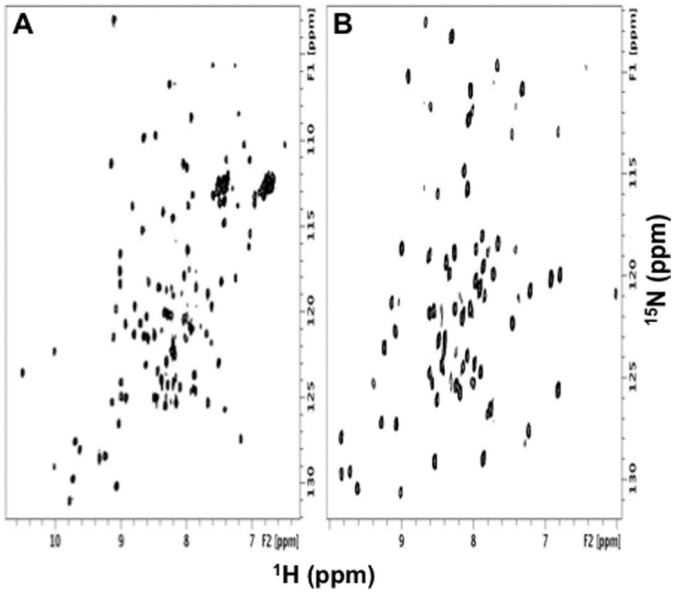

FIGURE 3. **NMR spectra showing that CD3$\epsilon\gamma$ and scFv-CD3$\epsilon\delta$ are folded.** *A*, two-dimensional ^{1}H-^{15}N HSQC spectrum of CD3$\epsilon\gamma$ with the γ-chain ^{15}N-labeled. *B*, two-dimensional ^{1}H-^{15}N TROSY HSQC spectrum of scFv-CD3$\epsilon\delta$ with the δ-chain ^{15}N-labeled. Conditions were as in Fig. 1.

The TCR β chain binding epitope thus identified by NMR is centered on the αA and αB helices, which are located at the base of the TCR (Fig. 5, *A* and *B*). This would position CD3$\epsilon\gamma$ and CD3$\epsilon\delta$ between the TCR and the T cell membrane, in agreement with the shorter length of the CD3 stalks compared with the TCR α and β chain stalks. The epitope is mainly hydrophilic, including the following solvent-accessible residues: Glu^{132}, Ser^{136}, His^{137}, Ser^{197}, Thr^{199}, Phe^{200}, Asn^{203}, Arg^{205}, Asn^{206}, and possibly also Trp^{240} and Arg^{242}. The surface area is relatively small (~400 Å^2), consistent with the weak interaction between TCR and CD3, although interactions from the α chain are as yet undetermined and may also contribute to binding with CD3. Importantly, the TCR β chain binding epitope is devoid of glycosylation sites, which are located well away from the αA/αB docking site with CD3.

A number of the residues undergoing chemical shift perturbations are not solvent-accessible and so cannot directly contact CD3. Notably, many of these are at the interface between the β and α chains of the MS2-3C8 TCR. Given that the chemical shift is an exquisitely sensitive measure of structure, these changes may reflect small adjustments in orientation between the α and β subunits due to cooperative binding of CD3$\epsilon\gamma$ and CD3$\epsilon\delta$. Even binding of CD3$\epsilon\gamma$ and scFv-CD3$\epsilon\delta$ individually to MS2-3C8 both appear to contribute to weak perturbations at the α/β-interface (*e.g.* Arg^{195} for scFv-CD3$\epsilon\delta$ and Val^{125}, Phe^{128}, and Ser^{131} for CD3$\epsilon\gamma$). If small domain rearrangements between the α and β chains of TCR are important, then it is possible that the non-native interchain disulfide between CαCys^{159} and CβCys^{171} may influence CD3 binding. Small long range effects like those seen here are commonly observed in chemical shift mapping of protein binding interactions (38).

Comparison of Binding Epitope with Mutational Data on TCR-CD3 Interactions—The docking site for CD3 on the TCR β chain identified by NMR (Fig. 5, *A* and *B*) may be compared with information on this site obtained from cell-based assays. In an extensive analysis of TCRβ-CD3 interactions, Fernandes *et al.* (20) mutated all Cβ residues whose side chains are >50% solvent-exposed and tested the effect of these mutations on surface expression of the TCR-CD3 complex in transduced Jurkat T cells lacking a functional TCR β chain. In Fig. 5, *C* and *D*, mutations in Cβ that reduced TCR expression by >60% compared with wild type are shown mapped onto the x-ray structure of MS2-3C8. Strikingly, both the NMR and cell-based approaches identified residues in the αA and αB helices as interacting with CD3. However, mutations that affected TCR surface expression were broadly distributed over the Cβ domain, in sharp contrast to the clustering of residues showing the largest chemical shift perturbations at the base of Cβ (Fig. 5, *A* and *B*). We conclude that the higher number of Cβ residues implicated by mutagenesis (20) than by NMR indicates that reduced TCR surface expression most likely reflects not only disruption of TCR-CD3 contacts but also deleterious effects on TCR folding, stability, and/or intracellular trafficking.

Impact of Mutations in the TCRβ-CD3 Interface on Cell Surface Expression—Finally, we assessed the importance of the TCRβ-CD3 interaction interface that we defined by NMR on TCR-CD3 cell surface expression. Because the key TCRβ residues at this interface are conserved between mice and humans (Val^{166}/Thr^{199}/Asn^{203}/Arg^{205}), we made non-conservative mutations in the H-2E^{k}-restricted, moth cytochrome *c* 88–102-specific AND TCR at these residues to determine whether this led to the disruption of the TCRβ-CD3 interaction. Multicistronic 2A-peptide-linked vectors were generated that contained the AND TCR$\alpha\beta$ with either a wild type or mutant TCRβ (TCRβ^{WT} or TCRβ^{Mut} (V166R, T199R, N203R, or R205E)), and an IRES.mAmetrine cassette to facilitate detection of transfectants by flow cytometry (26–29). Wild type or mutant AND TCR-encoding vectors were co-transfected with a similarly constructed multicistronic vector containing all four wild type CD3 chains (CD3ϵ^{WT}/CD3δ^{WT}/CD3ζ^{WT}/CD3γ^{WT}) that included an IRES-GFP cassette into HEK 293T cells. Cells were gated on GFP/mAmetrine, and the mean fluorescence of CD3ϵ and TCRβ was determined. A substantial reduction in TCR-CD3 expression (~66%) was reproducibly observed with TCRβ^{Mut}-*versus* TCRβ^{WT}-expressing cells (Fig. 7). These data suggest that this interface is required for optimal TCR-CD3 cell surface expression.

Discussion

We have demonstrated the feasibility of using NMR chemical shift mapping to define contacting surfaces between TCR and CD3 in solution, despite the low affinity of the interaction (K_D ~320 μM). An earlier NMR study did not detect binding between an unlabeled mouse TCR and ^{15}N-labeled CD3$\epsilon\delta$ (14). In fact, this result is consistent with our findings that the addition of unlabeled CD3$\epsilon\delta$ or CD3$\epsilon\gamma$ alone to MS2-3C8α[β-^{2}H,^{15}N] produced minimal chemical shift changes and that significant perturbations necessitated the addition of both CD3$\epsilon\delta$ and CD3$\epsilon\gamma$. This suggests that CD3 ECDs bind cooperatively to the TCR, in agreement with evidence from cell-based mutagenesis experiments that extracellular TCR-CD3$\epsilon\gamma$ interactions require TCR-CD3$\epsilon\delta$ interactions for stabilization (18). Coopera-

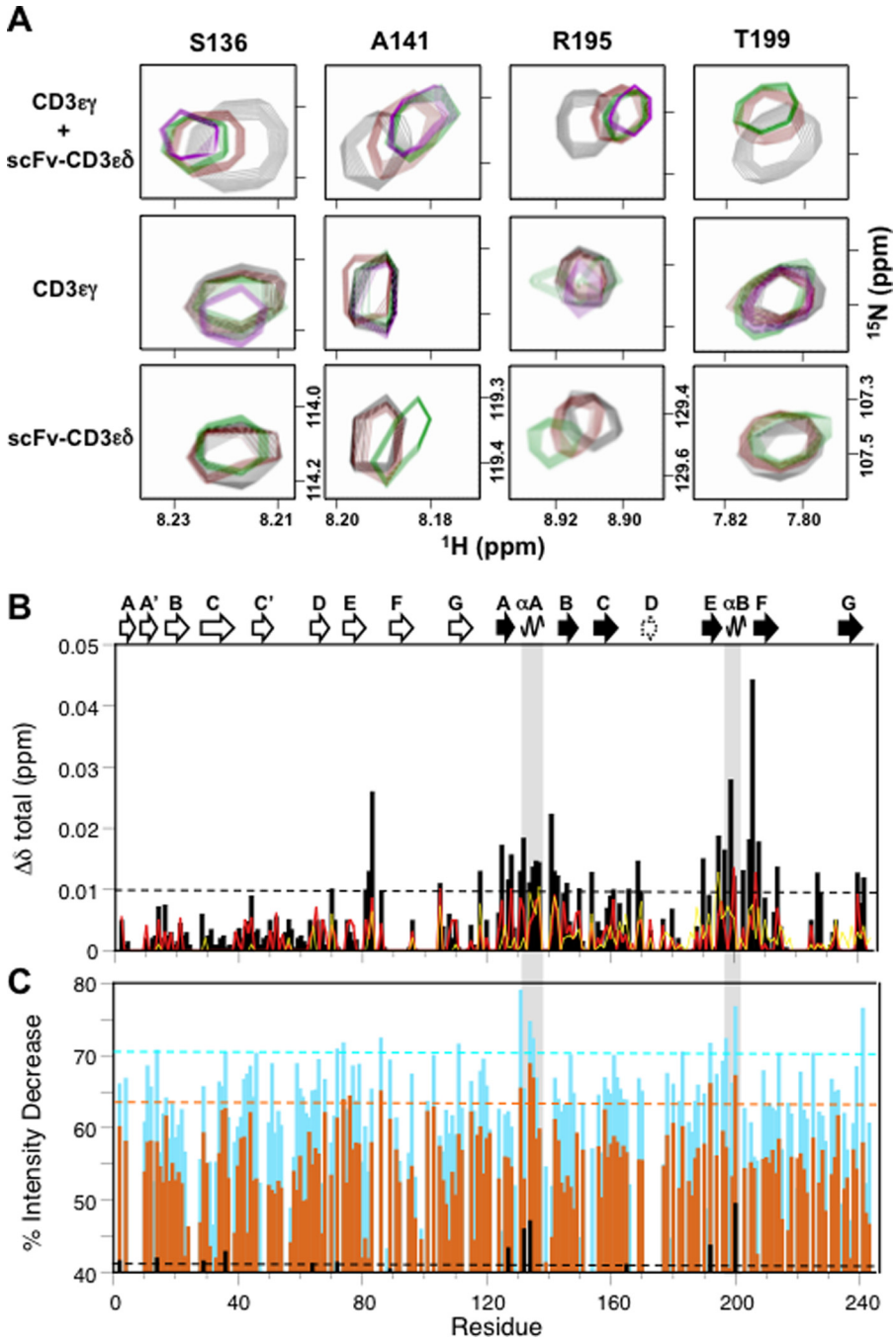

FIGURE 4. **Titration of TCR MS2-3C8α[β-^{2}H,^{15}N] with CD3.** *A*, (*top*) regions from two-dimensional ^{1}H-^{15}N TROSY HSQC spectra of MS2-3C8 with increasing amounts of CD3$\epsilon\gamma$ plus scFv-CD3$\epsilon\delta$. Molar ratios of MS2–3C8/CD3$\epsilon\gamma$/scFv-CD3$\epsilon\delta$ were as follows: MS2–3C8 alone (*black*), 1:2:2 (*red*), 1:4:4 (*green*), and 1:6:6 (*magenta*). *Center*, two-dimensional HSQC spectra of MS2–3C8 titrated with CD3$\epsilon\gamma$. Molar ratios of MS2–3C8/CD3$\epsilon\gamma$ are as follows: control (*black*), 1:2 (*red*), 1:4 (*green*), and 1:5.8 (*magenta*). *Bottom*, spectra of MS2–3C8 titrated with only scFv-CD3$\epsilon\delta$. Molar ratios of MS2–3C8/scFv-CD3$\epsilon\delta$ are as follows: control (*black*), 1:2 (*red*), and 1:3.3 (*green*). *B*, chemical shift perturbations ($\Delta\delta_{total}$) as a function of residue number for MS2-3C8 with CD3$\epsilon\gamma$ plus scFv-CD3$\epsilon\delta$ (*black*), CD3$\epsilon\gamma$ alone (*red*), and scFv-CD3$\epsilon\delta$ alone (*yellow*). Values *above* the *horizontal dashed line* are experimentally significant. *C*, the percentage decrease in intensity of MS2-3C8 amide peaks in two-dimensional HSQC spectra as CD3$\epsilon\gamma$ and scFv-CD3$\epsilon\delta$ are added together. The MS2-3C8/CD3$\epsilon\gamma$/scFv-CD3$\epsilon\delta$ molar ratios for peak intensity data are as follows: 1:2:2 (*black*), 1:4:4 (*orange*), and 1:6:6 (*cyan*). The corresponding *horizontal dashed lines* indicate the average value plus one S.D. value.

tivity could also arise from CD3$\epsilon\gamma$–CD3$\epsilon\delta$ interactions, although direct contacts between CD3 ECDs remain to be shown.

The CD3 docking site on Cβ, as defined here by NMR, comprises 9–11 residues that form a contiguous, mainly hydrophilic patch measuring ~400 Å^2. Assuming a total buried surface of ~800 Å^2 (2 × 400 Å^2), the TCRβ-CD3 interface would be below the lower limit of the average value of 1600 ± 400 Å^2 for stable protein-protein complexes, as defined by x-ray crystallography (39). However, it would be comparable in size with the interfaces of transient protein-protein complexes that mediate weak interactions in intracellular signaling or cell-cell adhesion (40). Although a variety of mechanisms have been proposed to explain TCR triggering, they all converge on the idea that TCR ligation somehow results in perturbation of the extracellular region of the TCR-CD3 complex through rigid body movements or intermolecular conformational changes

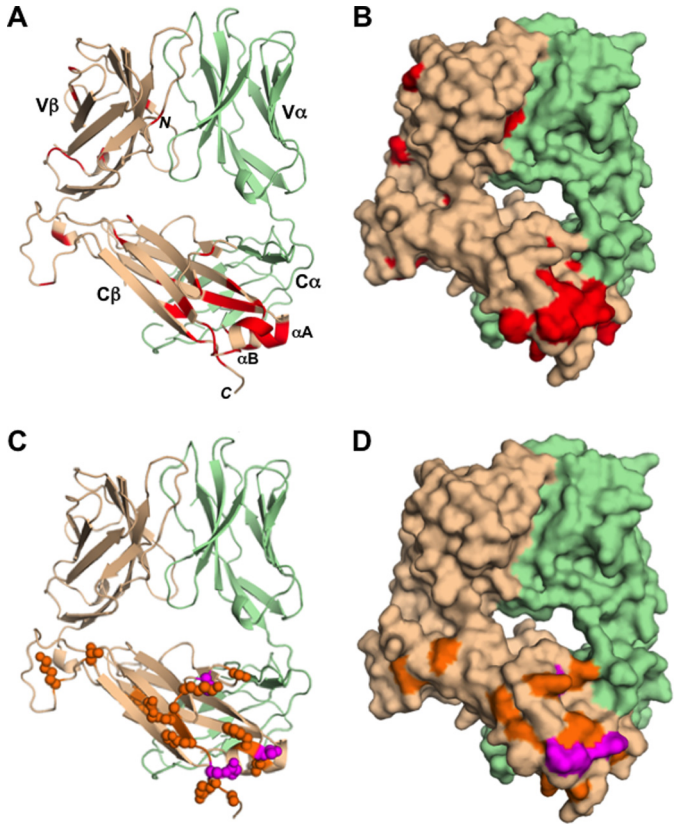

FIGURE 5. **The CD3 docking site on TCR MS2-3C8.** *A*, NMR chemical shift perturbations mapped onto the MS2-3C8 x-ray structure (Protein Data Bank code 3O6F). Values of $\Delta\delta_{total} \geq 0.01$ ppm from the titration of MS2-3C8α[β-^{2}H,^{15}N] with CD3εγ plus scFv-CD3εδ are indicated (*red*). *B*, *surface representation* of *A*. *C*, results from mutagenesis data obtained here (*magenta spheres*) and from Fernandes *et al.* (20) (*orange spheres*) mapped onto the MS2-3C8 structure with the same orientation as in *A*. Side-chain heavy atoms are highlighted for residues where mutation led to less than 60% TCR surface expression relative to wild type. *D*, *surface representation* of *C*.

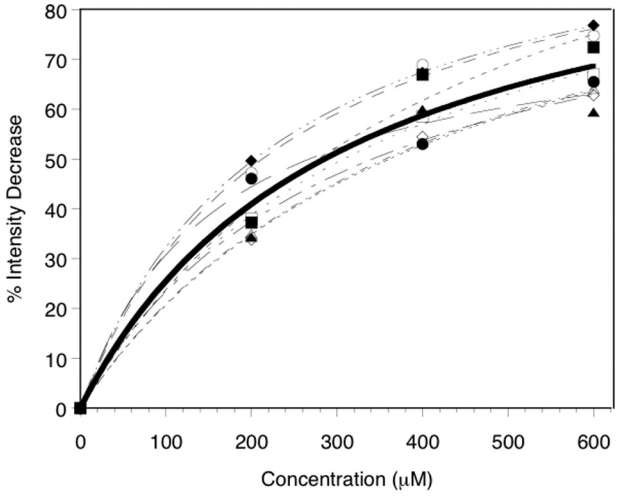

FIGURE 6. **Estimate of K_D for the TCR-CD3 interaction.** Plot of the percentage peak intensity decrease *versus* concentration of each CD3 in the titration of MS2-3C8 with CD3εγ and scFv-CD3εδ. Amide peak intensity changes are shown for αA and αB residues as follows: Glu^{132} (*filled circles*), Glu^{134} (*open circles*), Ile^{135} (*filled squares*), Ser^{136} (*open squares*), His^{137} (*filled triangles*), Thr^{199} (*open triangles*), Phe^{200} (*filled diamonds*), Asn^{203} (*open diamonds*). A *binding curve* is shown for each individual residue (*dashed lines*) and for the mean values (*bold line*).

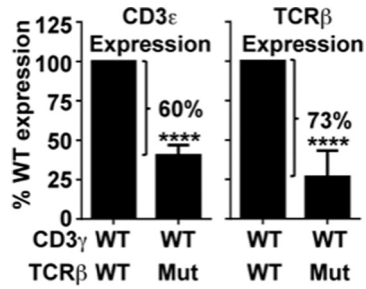

FIGURE 7. **Impact of structure-based mutations in TCRβ (V166R, T199R, N203R, and R205E) on surface expression of TCR-CD3 in transfected 293T cells.** HEK 293T cells were co-transfected with a multicistronic vector containing the AND-specific TCRα^{WT} with either TCRβ^{WT} or TCRβ^{Mut} (V166R, T199R, N203R, and R205E) and IRES-mAmetrine and a multicistronic vector containing CD3ε^{WT}/CD3δ^{WT}/CD3ζ^{WT}/CD3γ^{WT} and IRES-GFP. GFP^{+}/mAmetrine^{+} cells were gated, and the mean fluorescence of CD3ε and TCRβ was determined. The data were calculated as the percentage expression of WT. The data are the mean ± S.E. (*error bars*) of six independent experiments (****, $p < 0.0001$).

(10, 11, 17). In this regard, the weak and transient TCRβ-CD3 interaction revealed by our NMR analysis would facilitate shifts in the orientation of CD3 subunits with respect to TCR. By contrast, a more stable interaction mediated by a larger TCRβ-CD3 interface might rigidify the TCR-CD3 complex and thereby prevent effective T cell signaling. This hypothesis could be tested by engineering a high affinity TCRβ-CD3 interface through structure-guided mutagenesis.

We have shown that CD3 docks on the αA and αB helices of Cβ. This contact site positions CD3 at the base of the TCR, rather than alongside it, in agreement with results from SAXS and negative stain EM (22). As a consequence, CD3 would be situated between the TCR and T cell membrane, which is consistent with the greater length of the TCR α and β chain stalk regions (21 and 16 residues, respectively) than those of CD3εγ and CD3εδ (each ~9 residues). Mutational studies have demonstrated the importance of these highly conserved stalks for the assembly and function of the TCR-CD3 complex (41–45). Extension of our NMR analysis to the MS2-3C8 α chain will define the docking site for CD3 ECDs on the TCR more completely.

X-ray studies have shown that the ternary complex formed by MS2-3C8, MBP-HLA-DR4, and the CD4 co-receptor resembles a pointed arch in which TCR and CD4 are each tilted relative to the T cell membrane (Fig. 8) (32, 46). This structure, in conjunction with the location of the CD3 docking site established by NMR, places CD3εγ and CD3εδ inside the TCR-pMHC-CD4 arch, wedged between the TCR and T cell membrane and facing CD4 (Fig. 8). Importantly, this particular arrangement would achieve intracellular juxtaposition of CD3 ITAMs with the tyrosine kinase Lck bound to CD4, thereby promoting phosphorylation of CD3 ITAMs and T cell triggering.

Although virtually all regions of the MS2-3C8 β chain that were ordered in the NMR structure (high S^2 values) were also ordered in the x-ray structure (low *B* factors) (30), intriguing exceptions are the αA and αB helical regions that constitute the CD3 docking site. These α-helices are ordered in solution but display high *B* factors in the crystal. Whereas MS2-3C8 was bound to its pMHC ligand (MBP-HLA-DR4) in the x-ray structure, it was unbound in the NMR study. It is therefore tempting to speculate that binding of pMHC to the TCR could increase

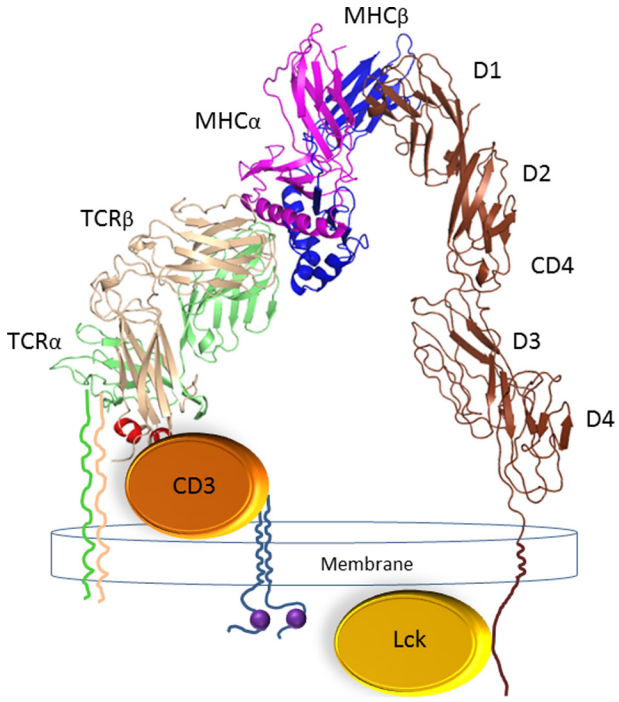

FIGURE 8. **Model of the TCR-CD3 complex bound to MHC and CD4.** Shown in a *ribbon representation* is the crystal structure of a TCR-pMHC-CD4 complex (MS2-3C8-MBP-DR4-CD4) oriented as if the TCR and CD4 molecules are attached to the T cell at the *bottom* and the HLA-DR4 MHC class II molecule is attached to an opposing antigen-presenting cell at the *top* (Protein Data Bank accession code 3TOE) (32). *Green*, TCR α chain; *wheat*, TCR β chain; *magenta*, MHC α chain; *blue*, MHC β chain; *brown*, CD4. *Highlighted* in *red* is the docking site for CD3 on the TCR β chain identified by NMR. The ectodomains of CD3 (*orange oval*) are wedged between the TCR and T cell membrane, opposite CD4. The tyrosine kinase Lck (*yellow oval*) is bound to the cytoplasmic tail of CD4. ITAMs on the cytoplasmic tails of CD3 subunits are drawn as *purple spheres*. The intracellular proximity of Lck to CD3 ITAMs promotes ITAM phosphorylation and T cell activation.

the flexibility of the CD3 docking site, thereby transmitting an allosteric signal from Vβ to Cβ and its associated CD3 subunits. Indeed, recent studies in several systems have demonstrated that ligand binding can alter protein flexibility at distant sites, resulting in long range transmission of biological signals, even in the absence of crystallographically observed structural changes (47–50). This process, known as dynamic allostery, is of special interest in cases such as the TCR, where x-ray crystallographic studies of multiple TCRs in free form and bound to pMHC have so far failed to identify clear and consistent conformational changes in the TCR Cα or Cβ domains that could be unambiguously attributed to antigen binding (4, 8, 10). Future studies will examine the possibility that MBP-HLA-DR4 ligation by MS2-3C8 induces allosteric changes in TCR dynamics that are transmitted to the CD3 signaling apparatus.

Author Contributions—Y. H., S. R., M. K., M. L., Y. C., Q. W., and Y. Y. expressed recombinant proteins and performed NMR experiments. C. J. W. and K. M. V. carried out mutational analysis. D. A. A. V., R. A. M., and J. O. wrote the manuscript.

References

1. Wucherpfennig, K. W., Gagnon, E., Call, M. J., Huseby, E. S., and Call, M. E. (2010) Structural biology of the T-cell receptor: insights into receptor assembly, ligand recognition, and initiation of signaling. *Cold Spring Harb. Perspect. Biol.* **2,** a005140
2. Kuhns, M. S., and Badgandi, H. B. (2012) Piecing together the family portrait of TCR-CD3 complexes. *Immunol. Rev.* **250,** 120–143
3. Call M. E., Pyrdol, J., and Wucherpfennig, K. W. (2004) Stoichiometry of the T-cell receptor-CD3 complex and key intermediates assembled in the endoplasmic reticulum. *EMBO J.* **23,** 2348–2357
4. Rudolph, M. G., Stanfield, R. L., and Wilson, I. A. (2006) How TCRs bind MHCs, peptides, and coreceptors. *Annu. Rev. Immunol.* **24,** 419–466
5. Marrack, P., Scott-Browne, J. P., Dai, S., Gapin, L., and Kappler, J. W. (2008) Evolutionarily conserved amino acids that control TCR-MHC interaction. *Annu. Rev. Immunol.* **26,** 171–203
6. Birnbaum, M. E., Dong, S., and Garcia, K. C. (2012) Diversity-oriented approaches for interrogating T-cell receptor repertoire, ligand recognition, and function. *Immunol. Rev.* **250,** 82–101
7. Yin, Y., Li, Y., and Mariuzza, R. A. (2012) Structural basis for self-recognition by autoimmune T-cell receptors. *Immunol. Rev.* **250,** 32–48
8. Rossjohn, J., Gras, S., Miles, J. J., Turner, S. J., Godfrey, D. I., and McCluskey, J. (2015) T cell antigen receptor recognition of antigen-presenting molecules. *Annu. Rev. Immunol.* **33,** 169–200
9. Samelson, L. E. (2002) Signal transduction mediated by the T cell antigen receptor: the role of adapter proteins. *Annu. Rev. Immunol.* **20,** 371–394
10. van der Merwe, P. A., and Dushek, O. (2011) Mechanisms for T cell receptor triggering. *Nat. Rev. Immunol.* **11,** 47–55
11. Kuhns, M. S., and Davis, M. M. (2012) TCR signaling emerges from the sum of many parts. *Front. Immunol.* **3,** 159
12. Sun, Z. J., Kim, K. S., Wagner, G., and Reinherz, E. L. (2001) Mechanisms contributing to T cell receptor signaling and assembly revealed by the solution structure of an ectodomain fragment of the CD3εγ heterodimer. *Cell* **105,** 913–923
13. Kjer-Nielsen, L., Dunstone, M. A., Kostenko, L., Ely, L. K., Beddoe, T., Mifsud, N. A., Purcell, A. W., Brooks, A. G., McCluskey, J., and Rossjohn, J. (2004) Crystal structure of the human T cell receptor CD3εγ heterodimer complexed to the therapeutic mAb OKT3. *Proc. Natl. Acad. Sci. U.S.A.* **101,** 7675–7680
14. Sun, Z. Y., Kim, S. T., Kim, I. C., Fahmy, A., Reinherz, E. L., and Wagner, G. (2004) Solution structure of the CD3εδ ectodomain and comparison with CD3εγ as a basis for modeling T cell receptor topology and signaling. *Proc. Natl. Acad. Sci. U.S.A.* **101,** 16867–16872
15. Arnett, K. L., Harrison, S. C., and Wiley, D. C. (2004) Crystal structure of a human CD3-ε/δ dimer in complex with a UCHT1 single-chain antibody fragment. *Proc. Natl. Acad. Sci. U.S.A.* **101,** 16268–16273
16. Call, M. E., Pyrdol, J., Wiedmann, M., and Wucherpfennig, K. W. (2002) The organizing principle in the formation of the T cell receptor-CD3 complex. *Cell* **111,** 967–979
17. Kuhns, M. S., Davis, M. M., and Garcia, K. C. (2006) Deconstructing the form and function of the TCR/CD3 complex. *Immunity* **24,** 133–139
18. Kuhns, M. S., and Davis, M. M. (2007) Disruption of extracellular interactions impairs T cell receptor-CD3 complex stability and signaling. *Immunity* **26,** 357–369
19. Kuhns, M. S., Girvin, A. T., Klein, L. O., Chen, R., Jensen, K. D. C., Newell, E. W., Huppa, J. B., Lillemeier, B. F., Huse, M., Chien, Y.-H., Garcia, K. C., and Davis, M. M. (2010) Evidence for a functional sidedness to the αβTCR. *Proc. Natl. Acad. Sci. U.S.A.* **107,** 5094–5099
20. Fernandes, R. A., Shore, D. A., Vuong, M. T., Yu, C., Zhu, X., Pereira-Lopes, S., Brouwer, H., Fennelly, J. A., Jessup, C. M., Evans, E. J., Wilson, I. A., and Davis, S. J. (2012) The T-cell receptor is a structure capable of initiating signaling in the absence of large conformational rearrangements. *J. Biol. Chem.* **287,** 13324–13335
21. Touma, M., Chang, H. C., Sasada, T., Handley, M., Clayton, L. K., and Reinherz, E. L. (2006) The TCR Cβ FG loop regulates αβ T cell development. *J. Immunol.* **176,** 6812–6823
22. Birnbaum, M. E., Berry, R., Hsiao, Y. S., Chen, Z., Shingu-Vazquez, M. A., Yu, X., Waghray, D., Fischer, S., McCluskey, J., Rossjohn, J., Walz, T., and Garcia, K. C. (2014) Molecular architecture of the αβ T cell receptor-CD3 complex. *Proc. Natl. Acad. Sci. U.S.A.* **111,** 17576–17581
23. Hyberts, S. G., Milbradt, A. G., Wagner, A. B., Arthanari, H., and Wagner, G. (2012) Application of iterative soft thresholding for fast reconstruction of NMR data non-uniformly sampled with multidimensional Poisson Gap

scheduling. *J. Biomol. NMR* **52,** 315–327
24. Delaglio, F., Grzesiek, S., Vuister, G. W., Zhu, G., Pfeifer, J., and Bax, A. (1995) NMRPipe: a multidimensional spectral processing system based on UNIX pipes. *J. Biomol. NMR* **6,** 277–293
25. Goddard, T. D., and Kneller, D. G. (2004) *SPARKY 3*, University of California, San Francisco
26. Holst, J., Wang, H., Eder, K. D., Workman, C. J., Boyd, K. L., Baquet, Z., Singh, H., Forbes, K., Chruscinski, A., Smeyne, R., van Oers, N. S., Utz, P. J., and Vignali, D. A. (2008) Scalable signaling mediated by T cell antigen receptor-CD3 ITAMs ensures effective negative selection and prevents autoimmunity. *Nat. Immunol.* **9,** 658–666
27. Holst, J., Szymczak-Workman, A. L., Vignali, K. M., Burton, A. R., Workman, C. J., and Vignali, D. A. (2006) Generation of T-cell receptor retrogenic mice. *Nat. Protoc.* **1,** 406–417
28. Holst, J., Vignali, K. M., Burton, A. R., and Vignali, D. A. (2006) Rapid analysis of T-cell selection *in vivo* using T cell-receptor retrogenic mice. *Nat. Methods* **3,** 191–197
29. Szymczak, A. L., Workman, C. J., Wang, Y., Vignali, K. M., Dilioglou, S., Vanin, E. F., and Vignali, D. A. (2004) Correction of multi-gene deficiency *in vivo* using a single "self-cleaving" 2A peptide-based retroviral vector. *Nat. Biotechnol.* **22,** 589–594
30. Yin, Y., Li, Y., Kerzic, M. C., Martin, R., and Mariuzza, R. A. (2011) Structure of a TCR with high affinity for self-antigen reveals the basis for escape from negative selection. *EMBO J.* **30,** 1137–1148
31. Quandt, J. A., Baig, M., Yao, K., Kawamura, K., Huh, J., Ludwin, S. K., Bian, H.-J., Bryant, M., Quigley, L., Nagy, Z. A., McFarland, H. F., Muraro, P. A., Martin, R., and Ito, K. (2004) Unique clinical and pathological features in HLA-DRB1*0401-restricted MBP 111–129-specific humanized TCR transgenic mice. *J. Exp. Med.* **200,** 223–234
32. Yin, Y., Wang, X. X., and Mariuzza, R. A. (2012) Crystal structure of a complete ternary complex of T-cell receptor, peptide-MHC, and CD4. *Proc. Natl. Acad. Sci. U.S.A.* **109,** 5405–5410
33. Pervushin, K., Riek, R., Wider, G., and Wüthrich, K. (1997) Attenuated T2 relaxation by mutual cancellation of dipole-dipole coupling and chemical shift anisotropy indicates an avenue to NMR structures of very large biological macromolecules in solution. *Proc. Natl. Acad. Sci. U.S.A.* **94,** 12366–12371
34. Tugarinov, V., Muhandiram, R., Ayed, A., and Kay, L. E. (2002) Four-dimensional NMR spectroscopy of a 723-residue protein: chemical shift assignments and secondary structure of malate synthase G. *J. Am. Chem. Soc.* **124,** 10025–10035
35. Wishart, D. S., and Sykes, B. D. (1994) The ^{13}C chemical-shift index: a simple method for the identification of protein secondary structure using ^{13}C chemical-shift data. *J. Biomol. NMR* **4,** 171–180
36. Boulter, J. M., Glick, M., Todorov, P. T., Baston, E., Sami, M., Rizkallah, P., and Jakobsen, B. K. (2003) Stable, soluble T-cell receptor molecules for crystallization and therapeutics. *Protein Eng.* **16,** 707–711
37. Shen, Y., Delaglio, F., Cornilescu, G., and Bax, A. (2009) TALOS+: a hybrid method for predicting protein backbone torsion angles from NMR chemical shifts. *J. Biomol. NMR* **44,** 213–223
38. He, Y., Chen, Y., Rozak, D. A., Bryan, P. N., and Orban, J. (2007) An artificially evolved albumin binding module facilitates chemical shift epitope mapping of GA domain interactions with phylogenetically diverse albumins. *Protein Sci.* **16,** 1490–1494
39. Lo Conte, L., Chothia, C., and Janin, J. (1999) The atomic structure of protein-protein recognition sites. *J. Mol. Biol.* **285,** 2177–2198
40. Nooren, I. M. A., and Thornton, J. M. (2003) Structural characteristics and functional significance of transient protein-protein interactions. *J. Mol. Biol.* **325,** 991–1018
41. Bäckström, B. T., Milia, E., Peter, A., Jaureguiberry, B., Baldari, C. T., and Palmer, E. (1996) A motif within the T cell receptor α chain constant region connecting peptide domain controls antigen responsiveness. *Immunity* **5,** 437–447
42. Xu, C., Call, M. E., and Wucherpfennig, K. W. (2006) A membrane-proximal tetracysteine motif contributes to assembly of CD3$\delta\epsilon$ and CD3$\gamma\epsilon$ dimers with the T cell receptor. *J. Biol. Chem.* **281,** 36977–36984
43. Martínez-Martín, N., Risueño, R. M., Morreale, A., Zaldívar, I., Fernández-Arenas, E., Herranz, F., Ortiz, A. R., and Alarcón, B. (2009) Cooperativity between T cell receptor complexes revealed by conformational mutants of CD3ϵ. *Sci. Signal.* **2,** ra43
44. Wang, Y., Becker, D., Vass, T., White, J., Marrack, P., and Kappler, J. W. (2009) A conserved CXXC motif in CD3ϵ is critical for T cell development and TCR signaling. *PLoS Biol.* **7,** e1000253
45. Brazin, K. N., Mallis, R. J., Li, C., Keskin, D. B., Arthanari, H., Gao, Y., Wu, S. L., Karger, B. L., Wagner, G., and Reinherz, E. L. (2014) Constitutively oxidized C*XX*C motifs within the CD3 heterodimeric ectodomains of the T cell receptor complex enforce the conformation of juxtaposed segments. *J. Biol. Chem.* **289,** 18880–18892
46. Li, Y., Yin, Y., and Mariuzza, R. A. (2013) Structural and biophysical insights into the role of CD4 and CD8 in T cell activation. *Front. Immunol.* **4,** 206
47. Smock, R. G., and Gierasch, L. M. (2009) Sending signals dynamically. *Science* **324,** 198–203
48. Tzeng, S. R., and Kalodimos, C. G. (2011) Protein dynamics and allostery: an NMR view. *Curr. Opin. Struct. Biol.* **21,** 62–67
49. Tzeng, S. R., and Kalodimos, C. G. (2012) Protein activity regulation by conformational entropy. *Nature* **488,** 236–240
50. Motlagh, H. N., Wrabl, J. O., Li, J., and Hilser, V. J. (2014) The ensemble nature of allostery. *Nature* **508,** 331–339